2021 43rd Annual International Conference of the
IEEE Engineering in Medicine & Biology Society (EMBC)
Oct 31 - Nov 4, 2021. Virtual Conference

# Properties of tissue within prostate tumors and treatment planning implications for ablation therapies

Natalie Beitel-White, *Graduate Student Member, IEEE*, Kenneth N Aycock, Navid Manuchehrabadi, Yajun Zhao, Khan Mohammad Imran, Sheryl Coutermarsh-Ott, Irving C Allen, Melvin F Lorenzo, Rafael V Davalos, *Member, IEEE*

***Abstract*—Irreversible electroporation (IRE) is a promising alternative therapy for the local treatment of prostate tumors. The procedure involves the direct insertion of needle electrodes into the target zone, and subsequent delivery of short but high-voltage pulses. Successful outcomes rely on adequate exposure of the tumor to a threshold electrical field. To aid in predicting this exposure, computational models have been developed, yet often do not incorporate the appropriate tissue-specific properties. This work aims to quantify electrical conductivity behavior during IRE for three types of tissue present in the target area of a prostate cancer ablation: the tumor tissue itself, the surrounding healthy tissue, and potential areas of necrosis within the tumor. Animal tissues were used as a stand-in for primary samples. The patient-derived prostate tumor tissue showed very similar responses to healthy porcine prostate tissue. An examination of necrotic tissue inside the tumors revealed a large difference, however, and a computational model showed that a necrotic core with differing electrical properties can cause unexpected inhomogeneities within the treatment region.**

***Index Terms*—electroporation, IRE, prostate cancer, treatment planning, urology**

## I. Introduction

Prostate cancer is the second-most common form of cancer among male adults and is most often diagnosed in men over the age of 65. Incidence rates are fairly high (over 1 million cases worldwide in 2018), and the five-year survival rate is 98% in the US [1]. The primary challenge in treating prostate tumors is preservation of anatomical structures. Irreversible electroporation (IRE) is a promising non-thermal therapy that can leave behind these anatomical structures while destroying tumor cells. The therapy involves inserting needle electrodes into the tumor, then applying high-voltage pulses on the order of 100 $\mu$s in duration. The ablation volume depends on parameters including electrode exposure and spacing, applied voltage, pulse shape and pulse frequency. These, along with a patient's unique anatomy, complicate treatment prediction. Computational models aim to provide a prediction, but these require material properties of the target zone to be known ahead of time. The zone may also contain both healthy and cancerous tissue, and possibly areas of necrosis.

This work was supported by AngioDynamics, Inc. N Beitel-White is with the Bradley Department of Electrical and Computer Engineering and Department of Biomedical Engineering and Mechanics at Virginia Tech, Blacksburg, VA, USA. KN Aycock, Y Zhao, MF Lorenzo, and RV Davalos are with the Department of Biomedical Engineering and Mechanics at Virginia Tech, Blacksburg, VA, USA. N Manuchehrabadi is with AngioDynamics, Inc., Latham, NY, USA. K Imran, S Coutermarsh-Ott, and I Allen are with the Department of Biomedical Sciences and Pathobiology at Virginia-Maryland College of Veterinary Medicine, Blacksburg, VA, USA.

## II. Background

Typical interventions for prostate cancer such as surgery and radiotherapy [2] carry a risk of damage to nearby anatomical structures, potentially resulting in complications such as erectile dysfunction and urinary incontinence. Non-thermal ablation modalities such as IRE allow for a more selective ablation, keep nearby structures intact and functional [3], and are not affected by thermal energy being carried away by blood flow [4], [5]. Results of clinical studies on the safety and efficacy of IRE are particularly promising for prostate cancer, with 5-year survival rates comparable to standard-of-care radical prostatectomy [6]. Joule heating is produced during pulsing, and the pulsing parameters ultimately determine whether thermal damage will occur. In addition to predicting an ablation for a given set of pulsing and electrical parameters, computational models can aid in avoiding thermal damage to structures. These models require the material properties of the tissue to be known; because electrical conductivity is electric-field dependent due to the nature of electroporation [7], a redistribution of the field occurs which is important to recapitulate for accurate prediction. These properties may be measured *ex vivo*, and a configuration which ensures a homogeneous electric field (EF) enables a simple calculation of conductivity for a given applied EF [7]. Primary tissue is preferable, but is limited in terms of volume. Pig tissue has been shown to accurately recapitulate human tissue [8] and thus is a useful substitute for normal prostate. For tumor tissue, patient-derived xenografts (PDX) have been shown to recapitulate the structures and features present in tumors while enabling large scale characterization and measurements [9]. The PDX model consists of excising a tumor and grafting it into the flank of an immunocompromised animal. The tumor will grow and eventually can be excised and expanded, resulting in larger total tissue volumes than samples excised from the original patient.

## III. Methods

### A. Animal Handling

Animals were handled according to the NIH Guide for the Care and Use of Laboratory Animals and all studies were

978-1-7281-1178-0/21/$31.00 ©2021 IEEE

approved by the Institutional Animal Care and Use Committee. For the prostate tissue, pigs were monitored for health before being sedated, then euthanized after 15 minutes or when fully sedated. NSGs each bearing a PDX on the right flank were ordered from Jackson Labs (TM00298 from Jackson's Mouse Tumor Biology Database). In total, 19 mice were used for the reported experiments. All mice were housed in immunocompromised conditions with autoclaved cage setups, autoclaved water, and irradiated chow. Mice were monitored three times weekly until tumors reached a size of 1-1.6 cm in tumor diameter as calculated by the square root of the product of diameters. Mice were euthanized by $CO_2$ asphyxiation, then secondary cervical dislocation.

### B. Experimental Setup

Experimental setup was identical to that reported previously in [10]. Briefly, tissue was placed in a modified phosphate-buffered solution immediately after removal from the animal. For each sample, a cylindrical piece was cut using a scalpel, then placed within a polydimethlysiloxane (PDMS) mold to retain the tissue in that shape (3 mm in diameter and 0.5-0.56 cm thick). All tissue was used within two hours from excision to maintain tissue integrity. The mold was then placed between two parallel-plate electrodes (BTX, Harvard Apparatus). All samples were then treated with a total of 100 pulses at 90 pulses per minute using a square pulse generator (ECM 830, Harvard Apparatus). Pulse width was 90 $\mu$s. Waveforms were captured using a high voltage probe and current probe connected to an oscilloscope (DPO2012, Tektronix). Conductivity was calculated as in equation (1) by averaging the last 5 $\mu$s of the current waveform, then calculating resistance according to Ohm's Law, and using the known cylindrical shape factor. Here, $l$ is the sample width, $R$ is the resistance and $A$ is the cross-sectional area of the sample.

$$\sigma = \frac{l}{R \cdot A} \tag{1}$$

For half of the porcine prostate samples, a 30 s delay was inserted every 25 pulses to gauge its effect on allowing heat to dissipate. An identical parallel-plate configuration was used for both pig and PDX tissue. Percent change in conductivity was calculated from raw values as % change = $100*(\sigma(E)-\sigma_{initial})/\sigma_{initial}$, where $\sigma_{initial}$ is the initial conductivity calculated from the 25 V pre pulse for that sample. Then, the average initial conductivity for all porcine prostate samples was calculated as $\sigma_{i,avg}$. Each conductivity value was then normalized and plotted versus applied EF magnitude by the relation $\sigma_{adjusted} = \sigma_{i,avg} * (1 + 0.01 * (\%\text{ change}))$. Finally, using the baseline temperature value for each sample, conductivity values were computed at 20 and 37 °C by assuming an increase of 2% in conductivity per °C. At least 5 samples were tested per EF magnitude. Conductivity data from the first pulse at each EF were then fit to equation (2).

$$\sigma(E) = \sigma_0 + \frac{\sigma_f - \sigma_0}{1 + e^{-A\cdot(E-E_{del})}} \tag{2}$$

### C. COMSOL Model

COMSOL Multiphysics 5.6 was used to construct a 3D shell model of a tissue domain containing three concentric spherical shells. The center shell was 1 cm in diameter, the middle shell was 1.6 cm in diameter, and the outer shell was assigned a diameter of 10 cm, large enough to avoid edge effects. The center shell was assigned a static conductivity value of 0.3 S/m to represent necrotic tissue; this was the mean value measured experimentally from the PDX tissue. The conductivity of the middle shell (tumor) was defined as a function of the spatial EF in the domain; the equation used matched the experimental results for PDX tissue reported in this paper. Similarly, the outer shell was assigned the measured dynamic conductivity function for normal porcine prostate tissue as reported in the next section. Two cylinders 1 mm in diameter were centered at the same point as the spheres, with a spacing of 1.5 cm and exposure length of 1.2 cm. The two domains were assigned properties of steel from the COMSOL materials library. The boundary of one cylinder was assigned an electric potential of 3000 V and the other was set to ground. A duty cycle approach was used to average the energy of 100, 90 $\mu$s electric pulses over 66.7 s (representing a frequency of 90 pulse per minute). First, a stationary solution was found for the electric potential distribution. Then, a time dependent simulation was performed for 100 s, which incorporated several heat sources: Joule heating, perfusion, and metabolism. The IT'IS database was used to find thermal properties for normal prostate tissue: thermal conductivity $k_p$, 0.51 W/(m·K); density $\rho_p$,1045 kg/m$^3$; specific heat $c_{pp}$, 3760 J/(kg·K); perfusion term $\omega_p$, 6.862E-3 1/s. Blood thermal properties used were: density $\rho_b$, 1050 kg/m$^3$; specific heat $c_{pb}$, 3760 J/(kg·K). A change in conductivity of 2% per °C was used. A physics-controlled mesh was generated using the "Coarse" setting in COMSOL, and was refined until the electric potential value in the center of the electrodes changed no more than 1%. This resulted in the use of the "Finer" mesh setting.

### D. Statistical Analysis

Prism software (GraphPad, v. 9.0.2) was used for all statistical tests; significance value was 0.05.

## IV. Results and Discussion

### A. Dynamic Conductivity Results

The 90 $\mu$s pre-pulse (25 V applied) was used to calculate initial conductivity for each sample point using the average current during the last 5 $\mu$s of the pulse. The mean initial conductivity across all 60 prostate samples was 0.21 S/m with a standard deviation of 0.043 S/m. The adjusted conductivity was calculated based on the percent change between the initial and high voltage conductivity value for each sample. The values fell within the range of those found in the literature for prostate [11]. As expected, prostate tissue demonstrated a sigmoidal conductivity dependence on the applied EF (Figure 1). Sigmoidal fit parameters for the adjusted conductivity data (Figure 2) at both 20 and 37 °C are shown in Table I.

When compared directly with the porcine prostate results, the conductivity values are similar for the PDX. This result could simplify computational modeling in prostate cancer IRE treatment plans. One reason for this phenomenon may be that overall, normal prostate tissue has a higher conductivity than other soft tissues such as pancreas, which was found to have a lower conductivity than PDX pancreas tissues [9], [10]. This creates a need for accounting for both tumor and normal properties in the appropriate tissue domains. In terms of electrical conductivity and temperature change, our data showed that the PDX tissues had very similar responses to that of the prostate. However, this conclusion is based on a single PDX tumor derived from one patient. To improve our confidence in these findings, additional patients should be added to this cohort to increase our statistical power.

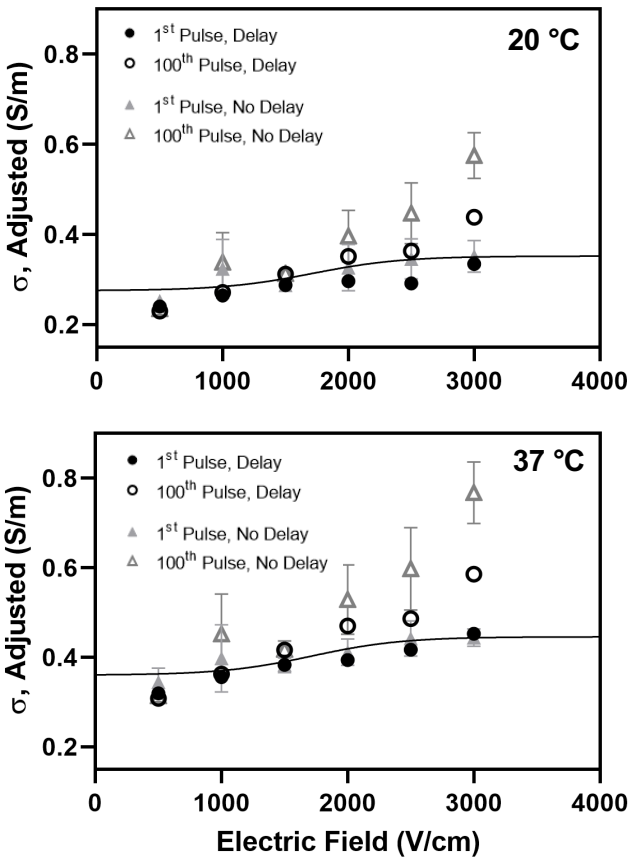


Fig. 1. **Adjusted IRE conductivity values and curve fits for porcine prostate tissue.** Using the average pre-pulse conductivity for all samples, the percent change from that average value was calculated. Then, the values were adjusted to either 20 or 37°C using the initial measured temperature.

TABLE I
CONDUCTIVITY DATA WERE FIT TO A SIGMOIDAL CURVE GIVEN BY EQUATION (2).

| **Temperature [°C]** | $\sigma_0$ **[S/m]** | $\sigma_f$ **[S/m]** | $A$ **[cm/V]** | $E_{del}$ **[V/cm]** |
|---|---|---|---|---|
| Porcine Prostate | | | | |
| 37 | 0.35 | 0.45 | 0.0028 | 1800 |
| 20 | 0.28 | 0.36 | 0.0028 | 1800 |
| PDX Prostate | | | | |
| 37 | 0.27 | 0.44 | 0.0029 | 1167 |
| 20 | 0.21 | 0.35 | 0.0029 | 1167 |

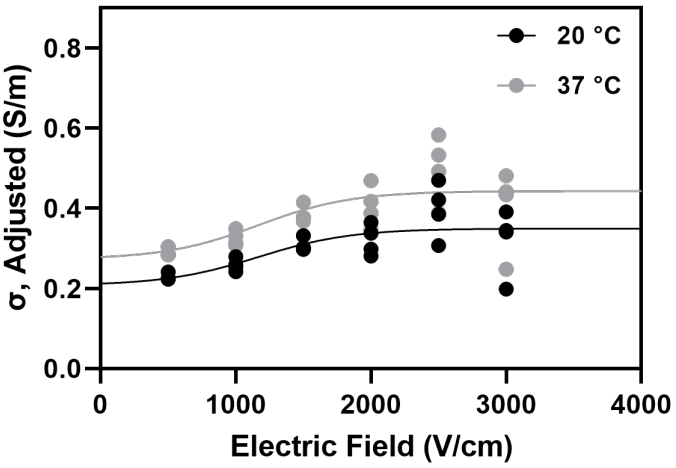


Fig. 2. **Adjusted IRE conductivity values and curve fits for IRE prostate PDX.** Raw electrical conductivity was calculated for each sample versus applied EF magnitude. The average initial conductivity for all porcine liver samples was calculated as $\sigma_{i,avg}$. Each conductivity value was adjusted and plotted versus applied EF magnitude by the relation $\sigma_{adjusted} = \sigma_{i,avg} * (1 + 0.01 * (\%\text{ change}))$. Then, using the baseline temperature value for each sample, conductivity values were computed at 20 and 37°C by assuming an increase of 2% in conductivity per °C. At least 5 samples were tested per EF magnitude. First pulse data were then fit to equation (2). Fit parameters are shown in Table I.

### *B. Necrotic Core versus Surrounding Tumor Tissue*

As IRE treatment plans aim to recapitulate patient anatomy and accurately predict the EFD, it is imperative that the appropriate electrical properties are taken into account. Many large tumors contain a centralized area of necrosis; as the tumor grows larger, the center dies, leaving behind a core of dead tissue. The spatial differences in conductivity were of interest, so four of the evaluated PDX tumors with particularly large necrotic cores were used to examine differences in impedance across the frequency spectrum (Figure 3) and in DC conductivity. For the necrotic core, the mean conductivity was 0.22 S/m with standard deviation of 0.037 S/m. For the surrounding tumor tissues, the mean conductivity was 0.16 S/m with standard deviation of 0.02 S/m. The results showed that impedance was significantly different between the two tissue types (paired t-test yielded for modulus: $p<0.001$; phase: $p=0.025$) while DC conductivity was not ($p=0.07$). More study is needed to determine whether this effect could have a marked impact on treatment plans for particularly large tumors with necrotic regions.

### *C. COMSOL Model Results*

The normal EF distribution was calculated and plotted (Figure 4). The difference in conductivity between the center shell (necrotic core) and middle shell (tumor) caused a higher EF to develop at the edges of the core domain. This effectively causes the EF contour around the electrodes to bend inward. In a prostate tumor treatment setting, because this bend occurs inside the tumor domain, the cells in that area could be

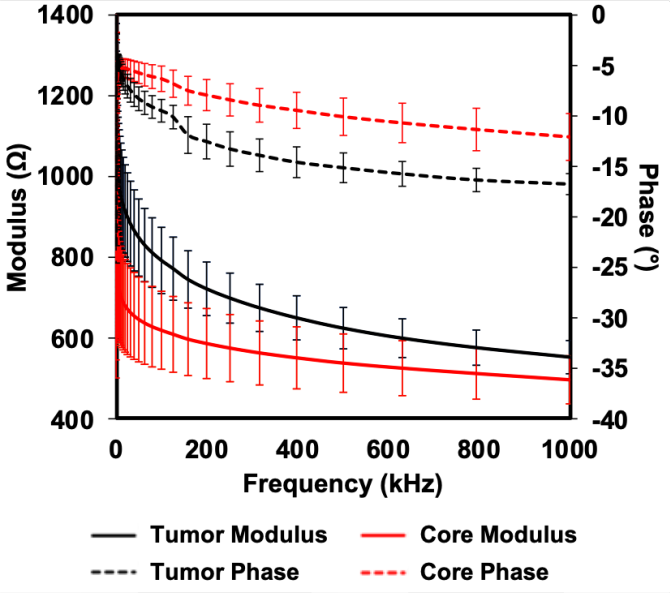


Fig. 3. **Necrotic core found to have lower impedance than surrounding tumor tissue.** For four PDX tumors with large necrotic cores, the center tissue was isolated from the surrounding tissue. Impedance was measured for each sample using a Gamry potentiostat.

exposed to a lower local electric potential than expected due to the presence of necrotic tissue nearby.

### *D. Limitations*

The reader should be aware of the limitations in the use of excised tissue; the data is based on measurements taken on tissue outside the body. Efforts were made to perform experiments within two hours of excision to prevent changes in tissue properties, but slight differences may occur. Additionally, the measurements were performed at ambient room temperature rather than body temperature. Finally, the reported results are expected to be fairly uniform in terms of sample-to-sample variability; in clinical practice, there is expected to be some patient-to-patient variability in electrical properties.

## V. Conclusions

Since IRE treatments depend heavily on the EF distribution within the target zone, it is important that tools and models incorporate the appropriate tissue properties for accurate prediction. Porcine prostate and PDX prostate tumor tissue were found to have similar conductivity behavior during IRE. However, examination of how necrotic tissue behaves in comparison suggests that unexpected inhomogeneities may occur in the EF distribution. This effect may be tissue-dependent, so more study is needed to determine how the necrotic core relates to other types of tumors in terms of electrical properties.

## Acknowledgment

N Beitel-White would like to acknowledge the Bradley fellowship from the Virginia Tech Department of Electrical and Computer Engineering for financial support.

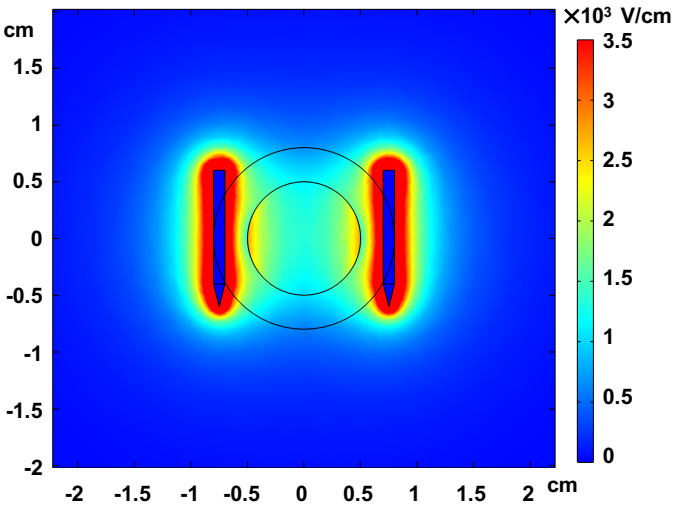


Fig. 4. **The norm of the EF was calculated and plotted in COMSOL for a typical two-needle electrode configuration and pulse parameters.** Because the three different concentric spherical domains were assigned differing conductivity values, edge effects can be seen in the EF magnitude at the boundaries between the domains.

## References

[1] P Rawla. Epidemiology of prostate cancer. *World journal of oncology*, 10(2):63, 2019.

[2] SM Noble, K Garfield, JA Lane, C Metcalfe, M Davis, EI Walsh, RM Martin, EL Turner, TJ Peters, and JC Thorn. The protect randomised trial cost-effectiveness analysis comparing active monitoring, surgery, or radiotherapy for prostate cancer. *British journal of cancer*, 123(7):1063–1070, 2020.

[3] E Guenther, N Klein, S Zapf, S Weil, C Schlosser, Boris Rubinsky, and MK Stehling. Prostate cancer treatment with irreversible electroporation (ire): Safety, efficacy and clinical experience in 471 treatments. *PloS one*, 14(4):e0215093, 2019.

[4] E Maor, A Ivorra, JJ Mitchell, and B Rubinsky. Vascular smooth muscle cells ablation with endovascular nonthermal irreversible electroporation. *J Vasc Interv Radiol*, 21(11):1708–15, 2010.

[5] LM Wu, LL Zhang, XH Chen, and SS Zheng. Is irreversible electroporation safe and effective in the treatment of hepatobiliary and pancreatic cancers? *Hepatobiliary Pancreat Dis Int*, 18(2):117–124, 2019.

[6] HJ Scheffer, K Nielsen, MC de Jong, A van Tilborg, JeM Vieveen, A Bouwman, S Meijer, C van Kuijk, P van den Tol, and MR Meijerink. Irreversible electroporation for nonthermal tumor ablation in the clinical setting: A systematic review of safety and efficacy. *Journal of Vascular and Interventional Radiology*, 2014.

[7] A Ivorra, LM Mir, and B Rubinsky. Electric field redistribution due to conductivity changes during tissue electroporation: experiments with a simple vegetal model. In *World Congress on Medical Physics and Biomedical Engineering, September 7-12, 2009, Munich, Germany*, pages 59–62. Springer, 2009.

[8] FA Duck. *Physical properties of tissues: a comprehensive reference book*. Academic press, 2013.

[9] RM Brock, N Beitel-White, S Coutermarsh-Ott, DJ Grider, MF Lorenzo, VM Ringel-Scaia, N Manuchehrabadi, RCG Martin, RV Davalos, and IC Allen. Patient derived xenografts expand human primary pancreatic tumor tissue availability for ex vivo irreversible electroporation testing. *Frontiers in Oncology*, 10:843, 2020.

[10] N Beitel-White, MF Lorenzo, Y Zhao, RM Brock, S Coutermarsh-Ott, IC Allen, N Manuchehrabadi, and RV Davalos. Multi-tissue analysis on the impact of electroporation on electrical and thermal properties. *IEEE Transactions on Biomedical Engineering*, 2020.

[11] P Hasgall, E Neufeld, and M Gosselin. IT'IS database for thermal and electromagnetic parameters of biological tissues, 2013.